Journal of Materials Chemistry A

Accepted Manuscript

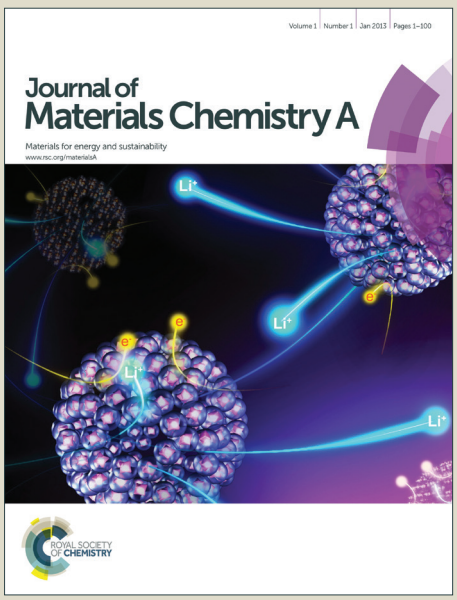

ROYAL SOCIETY OF CHEMISTRY

www.rsc.org/materialsA

Journal of Materials Chemistry A

Dynamic Article Links ►

Cite this: DOI: 10.1039/c0xx00000x

ARTICLE TYPE

www.rsc.org/xxxxxx

Carboxylate-intercalated Layered Double Hydroxides for H_2 Sorption

Yu-Wei Huang and Soofin Cheng*

Received (in XXX, XXX) Xth XXXXXXXXX 20XX, Accepted Xth XXXXXXXXX 20XX
DOI: 10.1039/b000000x

The Li-Al layered double hydroxides (LDHs) intercalated with two different arylate anions, terephthalate (TA) and *p*-toluate (*p*TA), and those mixed with acetate ions were prepared by one-pot co-precipitation method. The hydrogen storage capacities of the resultant LDHs and that intercalated with carbonate were examined. XRD patterns showed that all LDHs with different anion species had well-defined crystalline structures and the incorporation of organic anions was proved by IR spectra and thermal analysis. The surface areas and pore volumes of the LDHs increased when a portion of the interlayer arylate anions were replaced by acetate ions (aa^-). The adsorption enthalpies of LDHs toward H_2 varied with the interlayer anions and increased in the order of $pTA^- \sim aa^- < CO_3^{2-} < TA^{2-}$. However, the adsorption enthalpies became directly proportional to the micropore surface areas and volumes for LDHs containing mixed arylate and acetate ions. The latter materials also showed higher hydrogen uptakes than those intercalated with pure organic anions. Higher hydrogen uptakes were observed on TA-intercalated LDHs than *p*TA-intercalated LDHs. The maximal H_2 uptake per micropore surface area of the LDHs materials was higher than that of MOFs reported in the literature.

Introduction

Hydrogen is considered as a clean and efficient energy or alternative fuel because the only product formed in hydrogen combustion is water. The potential of utilizing hydrogen as the replacement for fossil fuels has led to immense researches in relating to its production, transportation, storage, and fuel cell technology. Among them, storage is one of the most challenging tasks for the development of hydrogen economy.[1] Storage systems revealed in the literature include high-pressure or liquefied hydrogen, metal hydrides, chemical hydrides, and porous adsorbents.[2,3] To store hydrogen in gas tanks at ambient temperature, 700 atm is needed for a compressed tank of a reasonable size, and the pressure is unacceptably high. To store hydrogen in the liquid form requires large energy consumption to achieve liquefaction at 20 K and it also suffers from the "boil-off" problem. Storage in metal and chemical hydrides involves chemical forces.[4] Thermodynamic and kinetic problems are of paramount importance in these systems because charging and discharging hydrogen involve the surface dissociation of hydrogen molecules and surface recombination of hydrogen atoms, which are both activated processes. The major disadvantage of these hydride materials is that the desorption temperature is over 573 K.[5,6] In the past decade, carbon materials,[7] metal organic frameworks (MOFs) [8,9,10,11,12] and other porous materials [13,14,15,16] have received considerable attention due to their high surface area for physisorption of hydrogen at 77 K. However, the hydrogen adsorption capacities at ambient temperature on all known sorbents are below 0.6-0.8 wt% at 298 K and 100 atm. From the materials reported in the literature, factors which could enhance the hydrogen storage capability through physisorption include surface area, pore volume, aromaticity[18], unsaturated metal sites[19], static charges, and increased enthalpy of adsorption. Up to now, it is still difficult to achieve the hydrogen storage criteria of U.S. department of energy (DOE), such as size, recharge ability, kinetics, cost, and safety requirements. In 2009, the U.S. DOE reset the storage target as 5.5 wt% and 40 g H_2/L at ambient temperature to achieve in 2015, mainly for on-board hydrogen storage in fuel cell applications in vehicles. The pressure is not specified, but 100 MPa has been a nominal pressure for research. For a compact passenger vehicle powered by fuel cell, 4 kg H_2 is needed for a driving range of 400 km. Metal-organic frameworks (MOFs) have been promising hydrogen storage materials. For example, the hydrogen uptake capacity of MOF-5, which has BET surface area of 3800 m^2/g and Langmuir surface area of 4400 m^2/g, is 7.1 wt% at 40 bar/77 K and 0.5 wt% at 100 bar/298 K.[20] MOF-5 constitutes metal cluster $(Zn_4O)^{6+}$ and organic linker (BDC^{2-}), where BDC^{2-} is 1,4-benzenedicarboylate or commonly named terephthalate (TA^{2-}). The drawback of MOF-5 is that its structure would collapse when the material was exposed in wet air.[21] Layered double hydroxides (LDHs) are known anionic clays with crystalline layer structures and may be converted to microporous materials through intercalation with various anionic pillars.[22,23] In this study, several factors which may affect hydrogen uptake, such as aromaticity, surface area, and pore volume were examined. Arylate anions, terephthalate (TA^{2-}) and *p*-toluate (*p*-TA^-), were chosen as intercalated anions to examine the influence

of aromaticity in H_2 uptake. The structural formulas of these arylate anions are depicted in Scheme 1. Besides, LDHs intercalated with carbonate and acetate of non-aromatic anions were also prepared for comparison.

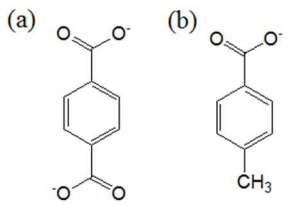

Scheme 1. Arylate anions incorporated in the interlayer of LDHs: (a) terephthate (TA^{2-}) and (b) *p*-toluate (*p*TA^-).

Experimental

Synthetic procedures

Generally, an aqueous solution of 0.05 mol $Al(NO_3)_3 \cdot 9H_2O$ in 125 mL distilled water was added dropwise to a 300 mL aqueous solution of LiOH (0.15 mol) and Na_2CO_3 (0.025mol) at room temperature under nitrogen atmosphere.[24] The mixture was stirred for 1 h at room temperature and aged for 18 h at 75~80°C. The resulting precipitate was centrifuged and washed with distilled water to pH~7 and the solids were dried at 323 K in air. The chemical formula of the resulting sample is $[Al_2Li(OH)_6(CO_3)_{0.5} nH_2O]$ or shortly named CO_3-LDH. In order to mimic MOF-5, interlayer carbonate was replaced by terephthalate, *p*-toluate ions, or the mixture of one of them with acetate. In addition, the arylate/acetate molar ratio was varied to increase surface area and pore volume. The molar ratios of reactant composition were 9 LiOH: $Al(NO_3)_3$: TA: (1-6) aa: 472 H_2O for the TA^{2-}-intercalated samples, which are named TA/*n*aa-LDH, where *n* is the molar ratio of aa/TA used in the synthesis solution. On the other hand, the molar ratios of reactant composition were 9 LiOH: $Al(NO_3)_3$: 1.5 *p*TA: (0.5-1.5) aa: 472 H_2O for the *p*-TA^--intercalated samples, which are named *p*TA/*n*aa-LDH, where *n* is the molar ratio of aa/*p*TA used in the synthesis solution.

Measurement

Powder X-ray diffraction (XRD) patterns were recorded in the 2-theta range of 3−70° using a Panalytical X'Pert PRO diffractometer with Cu Kα radiation (λ= 1.5418 Å) operating at 40 mA and 45 kV. Fourier-transform Infrared (FT-IR) spectra of the LDHs were measured on Bomem MB100 IR spectrophotometer using KBr pellets in the range of 550~4000cm^{-1}. The morphologies of the as-synthesized LDHs were examined by Hitachi S-800 Field Emission Scanning Electron Microscope (SEM). The thermo-gravimetric (TG) analysis was carried out on a TA Hi-Res TGA 2950 analyser under a 50 mL/min air flow. The metal content was determined with an inductive-coupled plasma-mass spectroscopy (Agilent 7700e ICP -MS instrument). The 10 mg sample was dissolved in a 40 mL of mixed HNO_3-HCl solution at room temperature overnight, and the solution was diluted 50-100 times prior to the measurement. Elemental analysis (C and H) were performed with thermo Flash 2000 instrument. Surface area and pore volume measurements were carried out by nitrogen physical sorption at liquid nitrogen temperature (77 K) with a Micromeritics Tristar 3000 instrument. Prior to the measurements, the sample was out-gassed overnight at 120°C under vacuum (10^{-3} Torr). The specific surface areas were determined using Brunauer-Emmett-Teller (BET) method in the P/P_0 range around 0.05–0.3. Single point total pore volumes were measured at P/P_0~0.95. Beside, the t-plot of the thickness and quantity of adsorbent was used to estimate the surface area and pore volume of micropores. The hydrogen adsorption isotherms measured at liquid nitrogen temperature (77 K) and liquid argon temperature (87 K) were using a Micromeritics Tristar 3000 system by volumetric method, and those at room temperature (298 K) were using a BEL MSB-AD-H system by gravimetric method. Prior to the measurements, the sample was out-gassed at 120°C for 3 h under vacuum (10^{-3} Torr).

Results and Discussion

Power X-ray diffraction

The structures of as-synthesized LDHs were examined by X-ray diffraction (XRD). Fig. 1A shows that the XRD pattern of carbonate product consists with the pattern of standard LDH ($Li_2Al_4(OH)_{12}(CO_3) \cdot 3H_2O$, JCPDS File Card No. 37-0728). The peaks at 2-theta angles of 11.84° and 23.72° correspond to the (003) and (006) diffraction planes, confirming the product with well-ordered layer structure. No impurity phases, such as LiOH and $Al(OH)_3$, were observed. The d-spacing of (003) plane (d_{003}) is similar for carbonate- and acetate-LDHs, and both are around 0.75 nm. Considering the thickness of gibbsite layer of 0.48 nm,[25] the gallery spacing is approximately 0.27 nm, indicating that carbonate and acetate anions are lying parallel to the gibbsite layers (Schemes 2A and 2B). On the other hand, the d_{003} values are 1.41 and 1.64 nm for terephthalate and *p*-toluate intercalated LDHs, respectively. By subtracting the thickness of gibbsite layer of 0.48 nm, the gallery spacings of TA^{2-} and *p*-TA^--intercalated LDHs are 0.93 and 1.16 nm, respectively. Since the length of the TA^{2-} anion is close to 0.9 nm,[26] the d_{003} value indicates that the TA^{2-}-intercalated LDH has TA^{2-} ions vertically arranged between the hydroxide layers. Because TA^{2-} is divalent and has two carboxylate groups, these carboxylate groups should attached to two different hydroxide layers and expand the layers apart (Scheme 2C). On the other hand, *p*-TA^- is monovalent and has only one carboxylate group to interact with the hydroxide layer. The d_{003} value of 1.64 nm for *p*-TA-intercalated LDHs infers that *p*-TA^- anions probably form bilayer in between the hydroxide layers with hydrophobic methyl groups facing toward the central section of the bilayer (Scheme 2D). If the two *p*-toluate layers expand head-to-head within the gallery, the height will be 1.8 nm.[24] The much shorter gallery spacing of *p*TA-LDH infers that the hydrophobic region of *p*-toluate anions should overlap strongly, probably through the π-π interaction between benzene rings.

For samples TA/*n*aa-LDH prepared with the mixture of TA^{2-} and acetate, the basal spacing retains at about 1.4 nm when $n = 1$, as shown in Fig. 1B. However, the strong diffraction peaks disappear and very weak diffractions appear at higher 2-theta angles when the molar ratios of aa/TA are higher than 2, implying the collapse of ordered arrangement of TA^{2-} expanded layered

structure. Moreover, the diffraction peaks further shift toward higher angles and some $Al(OH)_3$ phases appear with the further increase of *n* value to 6. The abrupt decrease of d-spacing from 1.41 nm to 1.08 nm when *n* value varied from 1 to 2 indicates that there is not enough amounts of interlayer TA^{2-} ions to stand vertically and expand the double-hydroxide layers. The gallery spacing of 0.6 nm implies that the TA^{2-} ions should tilt ca. 39° from the hydroxide surface. For TA/6aa-LDH, the d-spacing is lowered to 0.94 nm, resulting gallery spacing of 0.46 nm. This distance corresponds to a tilt angle of 29°. Nevertheless, the gallery spacing is roughly the size of benzene ring. Therefore, TA^{2-} ions should lie almost parallel to the hydroxide surface.

For samples *p*TA/*n*aa-LDHs prepared with the mixture of *p*-TA^- and acetate, an additional crystalline phase appears other than that of *p*TA-LDH (Fig. 1C). The d-spacings of the new layered structure vary in the range of 1.15- 1.22 nm. These values are close to the averaged d-spacings of *p*TA-LDH (1.64 nm) and aa-LDH (0.75 nm). Based on these analyses, the new phase should correspond to LiAl-LDHs intercalated with bilayer of mixed anions, with one acetate ion and one *p*-toluate ion facing each other through their hydrophobic sides. Furthermore, because of the strong π-π interaction between benzene rings, it is more likely that *p*-toluate ions would form one layer and acetate ions form another layer in the gallery (Scheme 2). This mixed bilayer structure becomes dominant when the molar ratio of aa/*p*-TA in the synthesis solution increases to 3.

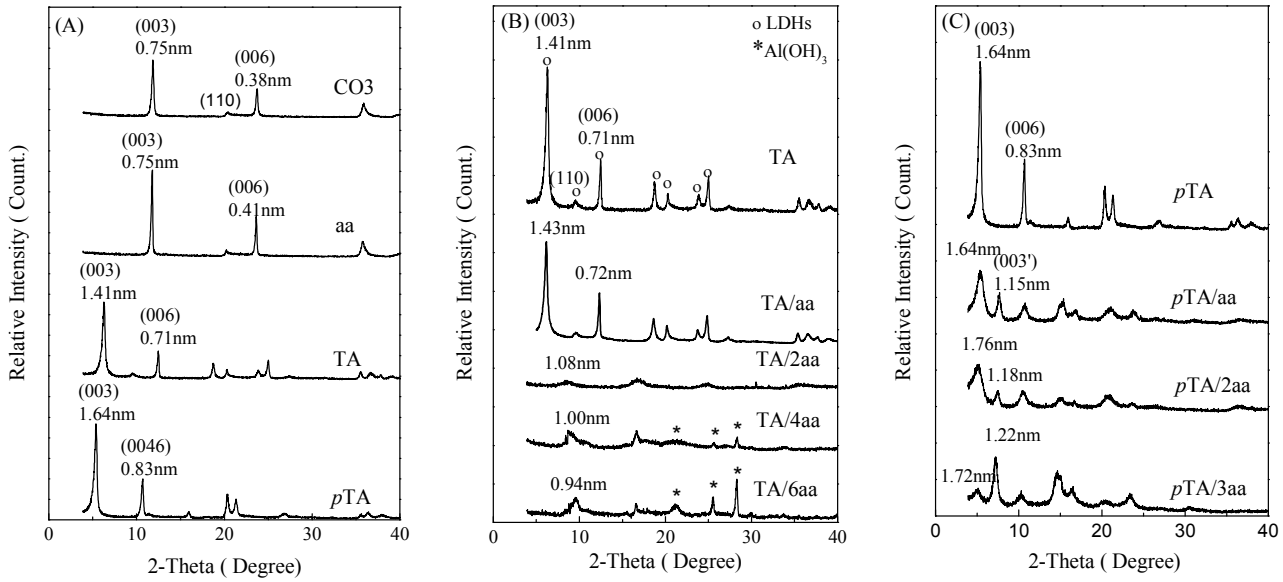

Fig. 1 XRD patterns of as-synthesized LiAl-LDHs (A) with different interlayer anions, (B) with the mixture of terephthalate and acetate, n= 0, 1, 2, 4 and 6, (C) with the mixture of *p*-toluate and acetate, n=1, 2, and 3.

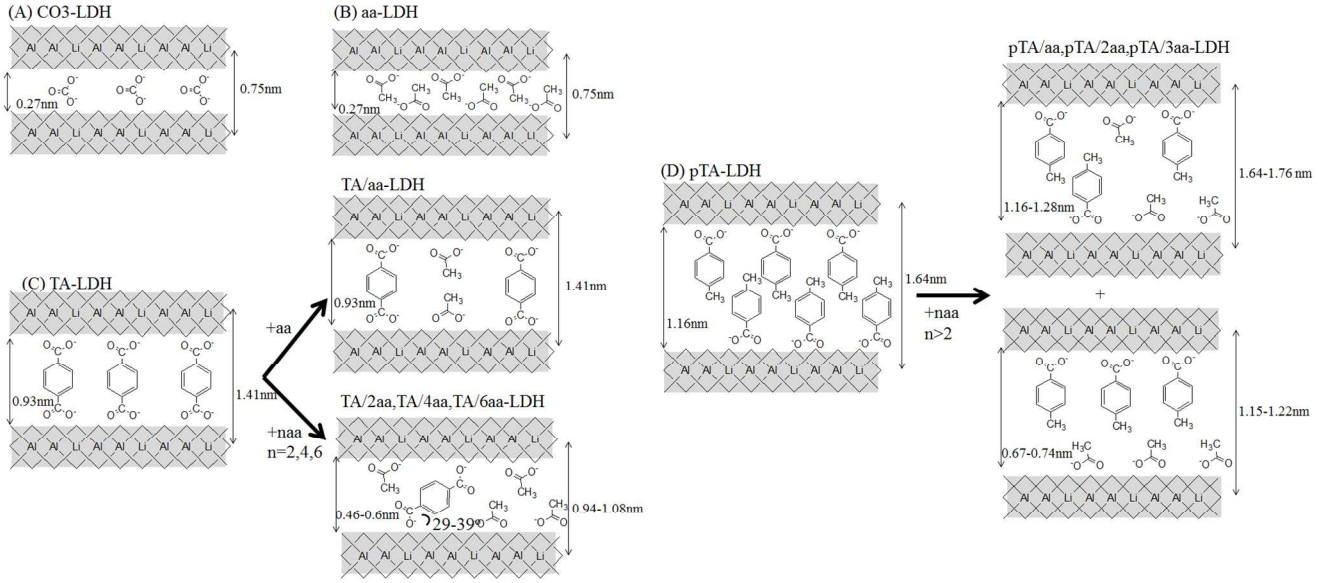

Scheme 2. The layer structures of LDHs intercalated with varied anions (A) CO_3-LDH (B) aa-LDH (C) TA/*n*aa-LDH, and (D) *p*TA/*n*aa-LDH.

To examine the hydrothermal stabilities of LDHs, the materials were exposed to a relative humidity of 90% at 323 K for 5 days. The XRD patterns of the samples after exposing to wet air are compared with those of original LDH samples, as shown in Fig. 2. The results indicate that the crystal structures of LDHs are well retained, implying that no dissolution or decomposition occurs upon exposure of LDHs to hot wet air.

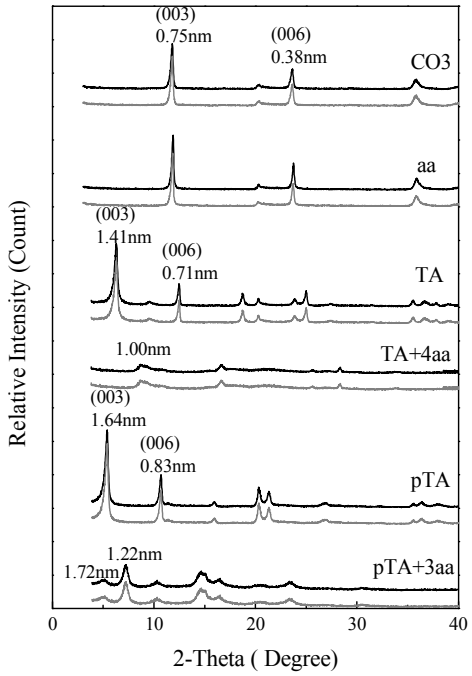

Fig. 2 XRD patterns the fresh LDHs (black) and LDHs (gray) after exposing at 323K and RH~90% for 5 days

Fourier-Transform Infrared (FT-IR) Spectra

The interlayer anions were confirmed by FT-IR spectra. Fig. 3A shows the broad band in the region of 3200-3600 cm^{-1}, which is associated with the O-H stretching vibration (υ_{OH}) of the OH groups in the gibbsite layer and those of the interlayer water with H-bonding. The bending vibration of the interlayer H_2O (δ_{H2O}) is shown in the broad bands around 1630 cm^{-1}. The band at about 1000 cm^{-1} is also associated with the vibrations of the hydroxyl groups which coordinate with the cations (Al^{3+} and Li^{+}) in the gibbsite layers.[27] In the low-frequency region, the sharp bands around 738 cm^{-1} are assigned to lattice O-M-O stretching vibrations ($\upsilon_{O\text{-}M\text{-}O}$), associated with metal hydroxide sheets.[28] For CO_3-LDH, the four absorption bands observed at 1375 (ν_3), 1068 (ν_1), 1000 (ν_2), and 680 (ν_4) cm^{-1} are assigned to the stretching vibration of the interlayer carbonate anion.[29,30] Fig. 3B shows the FT-IR spectra of TA/naa-LDHs samples. The stretching vibration of benzene ring ($\upsilon_{C=C}$) appears at 1570 cm^{-1}. The asymmetric and symmetric COO^- stretching vibrations of carboxylate anion appear at 1535cm^{-1} and 1390cm^{-1}, respectively. A sharp band at ~1385cm^{-1} is assigned to the stretching vibration of the interlayer NO_3^-. The IR spectra of *p*TA/*n*aa-LDHs are similar to but more complicated than those of TA/*n*aa-LDHs, as shown in Fig. 3C. The carboxyl and phenyl bands at 1588, 1532 and 1395 cm^{-1} are associated with *p*-toluate.

Scanning Electron Microscope (SEM)

The morphologies of LiAl-LDHs are examined by SEM, and the photographs are shown in Fig. S1 (ESI†). The samples intercalated with various anions are aggregates of particles. The morphologies of CO_3-LDH and aa-LDH are elliptical particles, as shown in Figs. S1(a) and S1(b) (ESI†). The particle sizes are around 100−120 nm for CO_3^{2-}-intercalated sample, and the sizes of aa-LDH are slightly smaller than those of CO_3-LDH.

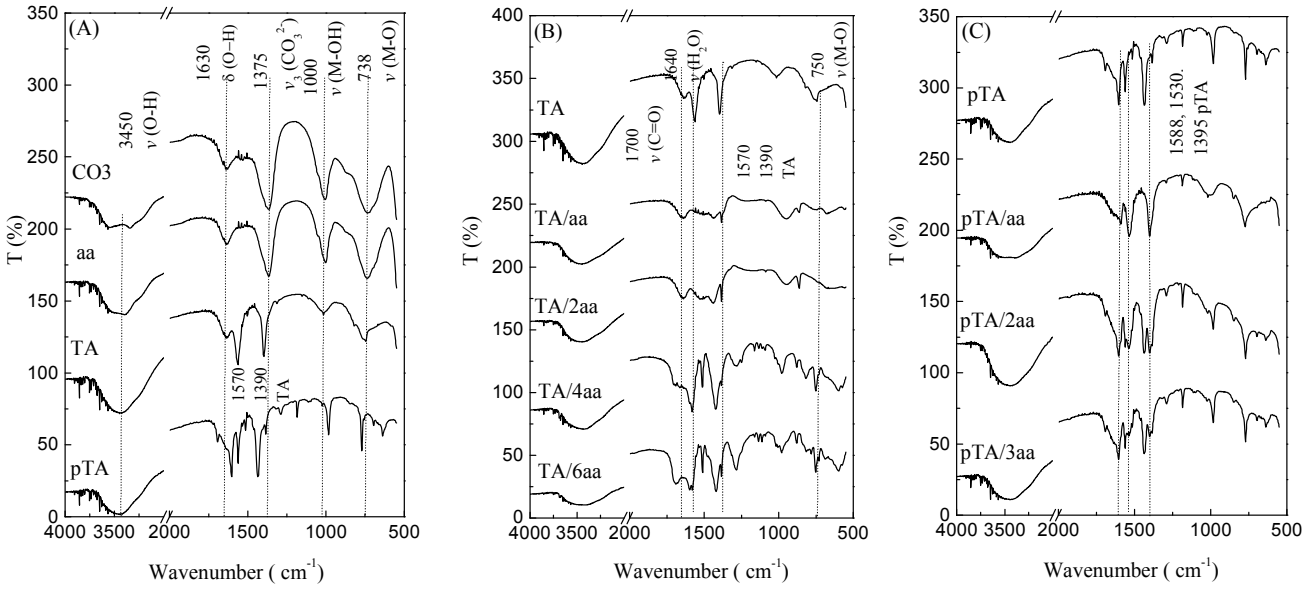

Fig. 3 FTIR spectra of as-synthesized LiAl-LDHs (A) with different interlayer anions, (B) with the mixture of terephthalate and acetate, n=0,1,2,4, and 6, (C) with the mixture of *p*-toluate and acetate, n= 1, 2, and 3.

Besides, the SEM images show that the morphologies of arylate intercalated LDHs are stacking of the hexagonal thin platelets. The thickness of these platelets is around several tens of nanometers and the lateral dimension is about 100−150 nm, as shown in Figs. S1(c) and S1(d) (ESI†). However, the morphologies of LDHs with a mixture of acetate and arylate are irregular blocks, which compose of nano-particles in several hundred nanometers (Figs. S1(e)−(k), ESI†). It implies that the acetate ions in the synthesis solution may disturb the intercalation of arylate into LDH.

Thermogravimetric analysis (TGA)

The compositions of LDHs with varied organic anions were examined by TGA under air flow, and the TG and the derivative (DTG) profiles are shown in Fig. S2 (ESI†). The CO_3-LDH and aa-LDH have weight losses in two stages (Fig. S2(a) and S2(b), ESI†). The first weight loss at temperature lower than 498 K is attributed to the water loss from internal gallery and the external non-gallery surfaces.[31] Because the samples are dried at 373 K overnight before TGA analyses and the outer surface areas of particles are relatively small, the contribution of non-gallery water is considered negligible. It is noticeable that the first weight loss of aa-LDH is much less than that of CO_3-LDH, indicating that acetate-intercalated LDH is more hydrophobic. The second weight loss at temperatures around 498−873 K involves dehydroxylation of the layers and loss of volatile species arising from decomposition of the interlayer carbonate and acetate anions. The shift of dehydroxylation temperature at second stage to higher temperature for aa-LDH indicates that aa-LDH is thermally more stable than CO_3-LDH. For arylate intercalated samples, the TGA and DTG profiles are shown in Fig. 4 and Fig. S3 (ESI†). Based on the DTG profiles, the weight losses can be divided into three decomposition steps. The interlayer water loss is below423 K for all samples. The decomposition of interlayer *p*TA$^-$ and TA^{2-} in TA-LDH and *p*TA-LDH occurs at higher temperatures than that of aa-LDH, implying that the carboxylate groups on TA and *p*TA are stabilized by the benzene ring. Moreover, TA-LDH with two carboxylate groups on each terephthalate ion attaching to two hydroxide layers has the highest thermal stability. Table 1 summarizes the results of elemental analyses by ICP and thermal analysis. The water weight losses in the first stage of the TG profiles for LDHs with different interlayer anions decrease in the order of CO_3> aa~ TA> *p*TA. These results indicate that carbonate ions are more hydrophilic than the organic anions. Between the two arylates-LDHs, *p*TA$^-$ with a methyl substitution on benzene is more hydrophobic than TA^{2-}.

For samples TA/*n*aa-LDH prepared with the mixture of TA^{2-} and acetate, the first weight loss increases from 17 wt% to 25 wt% when *n* is raised. It is attributed to that TA^{2-} is less hydrophilic than acetate. According to the XRD patterns (Fig. 1B), sample TA/6aa-LDH contains both the layer structure and $Al(OH)_3$ phases. $Al(OH)_3$ decomposes and transforms into *r*-Al_2O_3 at 523 K.[32,33] Therefore, the first weight loss of TA/6aa-LDH is 1.5 times higher than that of other TA/*n*aa-LDH samples. For samples *p*TA/*n*aa-LDH prepared with the mixture of *p*TA$^-$ and acetate, the first weight loss is significantly lower (in the range of 6-9 wt%). It is possible that the *p*TA$^-$ bilayer is closely stacked in the gallery, resulting in a very hydrophobic interlayer.

The weight losses of the second and third stages for CO_3-LDH and aa-LDH include dehydroxylation and anion decomposition. Assuming both LDHs have the same amounts of hydroxyl groups, the 14% excess weight loss of aa-LDH in comparison to that of CO_3-LDH is due to that a larger amount of acetate ions are needed to compensate the basal charges. Similarly, for arylate intercalated samples, the weight losses in this region of *p*TA-LDH is 16 wt% higher than that of TA-LDH because double amount of *p*TA$^-$ to TA^{2-} is necessary to balance the charges. It is noticeable that the weight losses for TA/*n*aa-LDHs containing a mixture of TA^{2-} and aa$^-$ are all around 41−43 wt%, except TA/6aa of 32 wt%. The XRD pattern (Figure 1B) shows that both the layer structure and $Al(OH)_3$ appear in TA/6aa sample. Therefore, the amounts of TA^{2-} and aa$^-$ intercalated into TA/6aa-LDH are less than the expected values. For pTA/*n*aa-LDH, the second and third weight losses are in the range of 47−55 wt%, the weight losses decrease gradually with the increase of acetate amount.

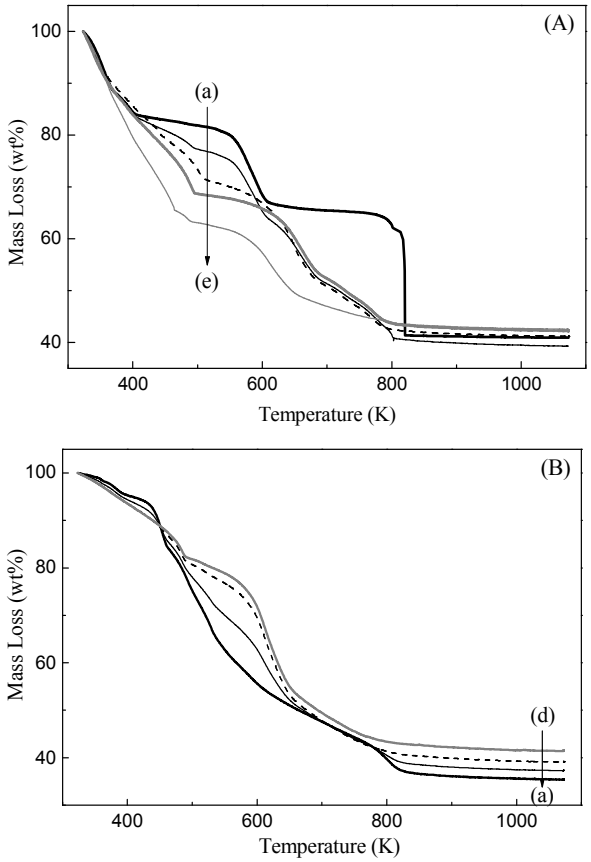

Fig. 4 TG-DTG profiles of LiAl-LDHs (A) TA/naa with n= (a)0, (b) 1, (c) 2, (d) 4, (e) 6, and (B) pTA/naa with n=(a)0, (b) 1, (c)2, and (d) 3.

Determination of the chemical formulas of LDHs

The matrix of LiAl-LDH is gibbsite, γ-$Al(OH)_3$. The host structure of gibbsite consists of stacking of sheets. Each sheet is formed by double layers of OH^- ions, in which the Al^{3+} ions occupy two-thirds of the octahedral holes. For LiAl-LDH, the Li^+ ions locate in the unfilled octahedral sites within the host

structure of gibbsite.[31] Therefore, the chemical formulas of LiAl-LDHs are in the form of $[Li_{2m}Al_2(OH)_6]^{(2m)+}[A_{2m/a}]^{a-}\ xH_2O$, where m is the Li/Al molar ratio and A is interlayer anion with a charge of $-a$. Accordingly, the formula of LDH intercalated with a mixture of TA^{2-} and aa^- ions can be written as $[Li_{2m}Al_2(OH)_6]^{(2m)+}[(TA)_a(aa)_b]^{(2a+b)-}\ xH_2O$, where $(2a+b) = 2m$, and that for LDH intercalated with a mixture of pTA$^-$ and aa^- ions is $[Li_{2m}Al_2(OH)_6]^{(2m)+}[(pTA)_a(aa)_b]^{(a+b)-}\ xH_2O$, where $(a+b) = 2m$. The Li/Al molar ratios (m) of the as-synthesized samples were determined by ICP-MS. The Li/Al molar ratios of CO_3-LDH and aa-LDH are close to the ideal value of 0.5, implying that all the vacant octahedral (O_h) sites of gibbsite are filled by Li^+ ions. However, those of pure arylate-intercalated LDHs are all less than 0.5, implying that the O_h vacancies of gibbsite structure are not completely filled by Li^+ ions. The interlayer anions are needed to balance the charge of the hydroxide layers, and the sum of the anion charges should be equal to the amount of Li^+ ions incorporated into the gibbsite. The lower Li/Al ratios observed on pure arylate-LDHs are attributed to that the arylate anions of larger sizes are probably more difficult to be intercalated into the interlayers in comparison to CO_3^{2-} and aa^- ions. For the samples intercalated with a mixture of arylate and acetate ions, the Li/Al molar ratio was found to increase with acetate amount and approach the ideal value of 0.5.

Elemental analyses of C and H in the samples were carried out by combustion analyses, and the results are shown in Table 1. The CO_3-LDH and aa-LDH have the C, H contents close to those derived from the proposed formulas. However, the C, H contents in arylate-intercalated samples are much higher than those derived from the formulas if only charge balance is considered. The only possible explanation for the high C, H contents is that some organic molecules are also incorporated in the interlayer of LDHs. This assumption should be reasonable because strong π-π interaction is present between these molecules and arylate ions. Accordingly; the formulas which satisfy charge balance as well as elemental analyses are derived based on the following equations:

For TA/$n$aa samples, $2a + b = 2m$

$[Li_{2m}Al_2(OH)_6]^{(2m)+}[(TA^{2-})_a(aa^-)_b]^{(2a+b)-}\ (TAH_2)_cxH_2O$

$$C = \frac{C*8*a+C*2*b+C*8*C}{Li*2m+Al*2+(OH)*6+TA*a+aa*b+(TAH2)*c+H2O*x} \qquad (eq.1)$$

$$H = \frac{H*6+H*4*a+H*3*b+H*6*c+H*2*x}{Li*2m+Al*2+(OH)*6+TA*a+aa*b+(TAH2)*c+H2O*x} \qquad (eq.2)$$

For pTA/$n$aa samples, $a + b = m$

$[Li_{2m}Al_2(OH)_6]^{(2m)+}[(pTA^-)_a(aa^-)_b]^{(a+b)-}\ (pTAH)c\ xH_2O$

$$C = \frac{C*8*a+C*2*b+C*8*C}{Li*2m+Al*2+(OH)*6+pTA*a+aa*b+(pTAH)*c+H2O*x} \qquad (eq.3)$$

$$H = \frac{H*6+H*7*a+H*3*b+H*8*c+H*2*x}{Li*2m+Al*2+(OH)*6+pTA*a+aa*b+(pTAH)*c+H2O*x} \qquad (eq.4)$$

where, "C" and "H" represent the mass ratios of carbon and hydrogen in the LDHs.

As shown in Table 1, the amount of acetate ions intercalated into the interlayer of LDHs increases with that introduced in the synthesis solutions. The empirical n value is obtained by b/a from the derived formula. Nevertheless, the n values are much higher than the values started with in the synthesis solutions, implying that small acetate ions are favourable to arylate ions in incorporation to LDHs. Since each interlayer acetate ion brings in one Li^+ ion to the Gibbsite layer, more Li^+ ions are incorporated in the Gibbsite layer as well. It is also noticed that the amount of organic molecules incorporated in the interlayer is much higher than that of arylate ions. Moreover, that varies in a similar trend as the amount of acrylate ions and also decreases with the increase in acetate content. This result confirms that π-π interaction between the organic molecules and arylate ions is the driving force for the incorporation of the neutral molecules into the interlayer of LDHs.

Table 1. The results of elemental analyses by ICP and TGA.

Interlayer species	Li/Al[a] (m)	1st wt. loss (%)[b] (Temp. range)	2nd+3rd wt. loss (%)[b]	C (%)[c]	H (%)[c]	Formal	n[e]
CO_3	0.51	26 (323-498 K)	26	3.2	4.1	$[Li_{1.02}Al_2(OH)_6][CO_3^{2-}]_{0.51}1.50H_2O$ C= 2.8%; H= 4.1% [d]	–
aa	0.53	18 (323-498 K)	40	10.8	4.0	$[Li_{1.06}Al_2(OH)_6][CH_3COO^-]_{1.06}0.02H_2O$ C= 11.2%; H= 4.0%	–
TA	0.37	17 (323-423 K)	42	40.2	3.4	$[Li_{0.74}Al_2(OH)_6][C_6H_4(COO^-)_2]_{0.37}[C_6H_4(COOH)_2]_{1.89}0.16H_2O$ C= 40.3%; H= 3.4%	–
TA/aa	0.43	18 (323-423 K)	43	37.3	3.6	$[Li_{0.86}Al_2(OH)_6][C_6H_4(COO^-)_2]_{0.26}[C_6H_4(COOH)_2]_{1.54}[aa]_{0.34}0.25H_2O$ C= 37.3%; H= 3.7%	1.3
TA/2aa	0.46	17 (323-423 K)	41	29.9	3.8	$[Li_{0.92}Al_2(OH)_6][C_6H_4(COO^-)_2]_{0.15}[C_6H_4(COOH)_2]_{0.84}\ (aa)_{0.62}0.28H_2O$ C= 29.9%; H= 3.8%	4.1
TA/4aa	0.53	19 (323-423 K)	41	22.5	4.1	$[Li_{1.06}Al_2(OH)_6][C_6H_4(COO^-)_2]_{0.08}[C_6H_4(COOH)_2]_{0.42}(aa)_{0.90}0.58H_2O$ C= 22.5%; H= 4.1%	11.3
TA/6aa	0.51	25 (323-423 K)	32	15.0	4.3	$[Li_{1.02}Al_2(OH)_6][C_6H_4(COO^-)_2]_{0.02}[C_6H_4(COOH)_2]_{0.14}[aa]_{0.98}0.69H_2O$ C= 15.0%; H= 4.3%	49
pTA	0.39	6 (323-423K)	58	55.9	4.9	$[Li_{0.78}Al_2(OH)_6][C_7H_7(COO^-)]_{0.78}[C_7H_7COOH]_{3.81}0.15H_2O$ C= 55.9 %; H= 5.4%	–
pTA/aa	0.60	7 (323-423 K)	55	41.6	5.0	$[Li_{1.20}Al_2(OH)_6][C_7H_7(COO^-)]_{0.42}[C_7H_7COOH]_{1.39}[aa]_{0.60}0.36H_2O$ C= 41.6%; H= 4.1%	1.4
pTA/2aa	0.52	9 (323-423 K)	52	28.6	5.3	$[Li_{1.04}Al_2(OH)_6][C_7H_7(COO^-)]_{0.18}[C_7H_7COOH]_{0.91}[aa]_{0.86}4.26H_2O$ C= 28.6%; H= 5.3%	4.8
pTA/3aa	0.30	9 (323-423 K)	47	24.3	5.1	$[Li_{0.60}Al_2(OH)_6][C_7H_7(COO^-)]_{0.08}[C_7H_7COOH]_{0.65}[aa]_{0.52}2.73H_2O$ C= 24.3%; H= 5.1%	6.5

[a] The metal atomic molar ratio (m) is determined by ICP-MS. [b] The mass loss of thermal decomposition is determined by TGA. [c] C and H contents determined by EA. [d] C, H contents based on the formula. [e] The n value is the aa/arylate ratio in the formula.

Surface area and pore volume analysis

The nitrogen sorption isotherms and the BJH pore size distribution (PSD) profiles calculated based on the desorption profiles are shown in Fig. S4 (ESI†). The materials intercalated with pure anions display similar type IV isotherms with parallel H1 type hysteresis loops appeared in the high relative pressure of 0.9-1.0, while the samples containing mixed arylate and acetate ions have type H2 hysteresis loops appeared at lower P/P_0. The increases in amounts of N_2 sorption at high P/P_0 correspond to pores formed by aggregation of nano particles. On the other hand, the PSD profile of TA/4aa-LDH exhibits a narrow size distribution with the maximum at 3.6 nm. Although *p*TA/3aa-LDH also presents a narrow peak in the PSD profile at ca. 3.8 nm, the N_2 uptake is very low and the corresponding pore volume should be negligible. These results indicate that mixing acetate ions with arylates in intercalation of LDHs can generate both micropores and mesopores. The micropores are arisen from the replacement of interlayer arylate ions (ca. 0.9 nm in length) by the smaller acetate ions (0.27 nm), as shown in Scheme 2. On the other hand, the mesopores are formed by aggregation of nano particles, which are a result of disturbance of the precipitation by the acetate ions. The SEM images in Fig. S1 (ESI†) confirm that the particles of LDHs intercalated with pure arylate ions are generally larger than those with mixed acetate and arylate.

The textural properties derived from the N_2 sorption isotherms of the layered double hydroxides are listed in Table 2. The micropore surface areas and volumes are estimated using t-plot method, and the mesopore surface areas and volumes are obtained by subtracting the micropore contribution from the total values. The BET surface areas of LDHs intercalated with pure anions are very low, in the range of 19−47 m^2/g, and the total pore volumes are in 0.03−0.08 cm^3/g. The pure organic anions intercalated LDHs have lower surface areas and pore volumes than those of CO_3-LDH. The lowest surface area of *p*TA-LDH should be elucidated by the close-packed pTA^- ions forming bilayer arrangement in between the hydroxide layers through π-π interaction. The packing of benzene rings in TA-LDH should be relaxed due to that each TA^{2-} ion is divalent and a half amount of benzene rings is needed to balance the charge in comparison to *p*TA-LDH. Indeed, the surface area and pore volume of TA-LDH are higher than those of *p*TA-LDH for ca. 30% and 67%, respectively.

Enormous increases in the surface area and pore volume can be achieved by replacing a portion of the interlayer arylate anions by acetate. The BET surface areas raise from 25 m^2/g to 50-138 m^2/g for TA/*n*aa-LDHs and from 19 m^2/g to 22-166 m^2/g for *p*TA/*n*aa-LDHs. The total pore volumes also increase up to 4.6 and 6 times higher than those of pure arylate-LDHs. Table 2 show that all the materials contain both the micro- and meso-pore surface areas and volumes. It is also noticeable that the mesopore surface areas (S_{meso}) and volumes (V_{meso}) are generally higher than the micropore surface areas (S_{micro}) and volumes (V_{micro}). Nevertheless, TA/*n*aa-LDHs samples contain largest S_{micro}, while *p*TA/3aa-LDH contains the largest S_{meso}. These results demonstrate that intercalating LDHs with a mixture of TA^{2-} and acetate ions is more effective in generating micropores than that with a mixture of pTA^- and acetate ions. On the other hand, the exceptionally large S_{meso} of *p*TA/3aa-LDH is due to the formation of two separated layered phases. The notably large S_{micro} values of TA/*n*aa-LDHs samples with $n = 4, 6$ are likely attributed to the interlayer voices formed by tilted TA^{2-} ions and acetate.

H_2 uptake

The hydrogen uptakes of LDH materials intercalated with different anions were measured at 77 K up to 1 atm pressure via volumetric method and also under high-pressure up to 100 atm at room temperature by gravimetric method. The H_2 absorption isotherms at 77 K are shown in Fig. 5, and the uptakes at the maximum pressure are shown in Table 2. All the absorption profiles belong to Langmuir isotherms. LDHs containing mixed arylate and acetate ions apparently have higher hydrogen uptakes than those with pure anions at 77 K and 1 atm.

Table 2. Textural properties and hydrogen uptakes of LDHs with different anions.

Interlayer species	Surface area (m^2/g)			Pore volume (cm^3/g)			Hydrogen Uptake		
	S_{BET}	S_{micro} [a]	S_{meso} [b]	V_{total}	V_{micro} [a]	V_{meso} [c]	77 K, 1 atm (wt%)	$-Q_{ads}$ [d] (kJ/mol)	298 K, 100 atm (wt%)
CO_3	47	14	33	0.08	0.015	0.065	0.13	5.7	0.024
aa	36	3	33	0.06	0.008	0.052	0.03	4.8	0.007
TA	25	4	21	0.05	0.007	0.043	0.05	8.3	0.005
TA/aa	50	7	43	0.06	0.011	0.049	0.06	8.8	0.009
TA/2aa	105	11	94	0.10	0.013	0.087	0.10	9.9	0.015
TA/4aa	126	73	53	0.13	0.047	0.083	0.68	21.2	0.098
TA/6aa	138	52	86	0.23	0.034	0.196	0.47	15.3	0.068
*p*TA	19	3	16	0.03	0.005	0.025	0.03	4.5	0.004
*p*TA/aa	22	5	17	0.04	0.007	0.033	0.05	5.7	0.010
*p*TA/2aa	53	13	40	0.13	0.016	0.114	0.12	8.4	0.024
*p*TA/3aa	166	30	136	0.18	0.023	0.157	0.28	13.6	0.071

[a] The S_{micro} and V_{micro} are calculated by t-plot method. [b] calculated by S_{total}-$S_{micro.}$ [c] calculated by V_{total}-V_{micro}.
[d] Q_{ads} values calculated at zero coverage by Clausius-Clapeyron equation.

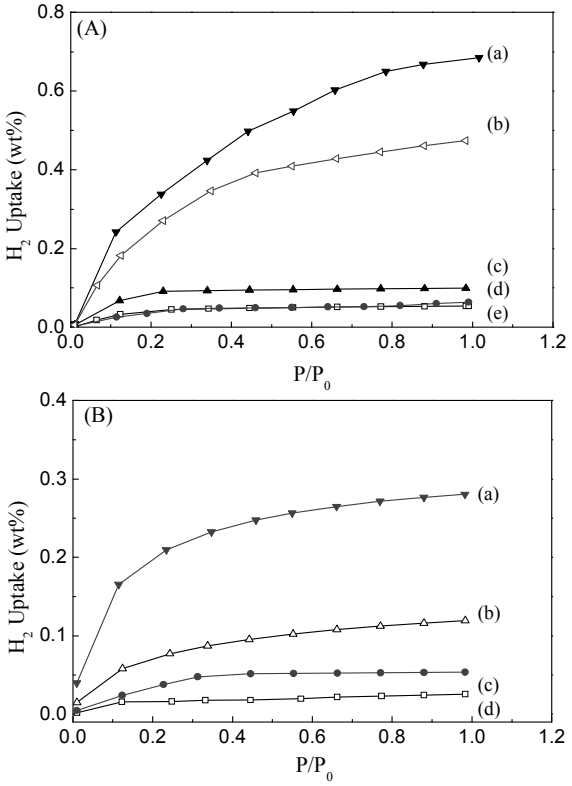

Fig. 5 H_2 adsorption isotherms of LiAl-LDHs with different interlayer anions at 77K and 1 atm (A) TA/*n*aa (a) n=4,(b) 6, (c) 2, (d) 1, (e) 0, and (B) *p*TA/*n*aa (a)*n*=3, (b) 2, (c) 1(d) 0.

Among LDHs containing mixed arylate and acetate ions, TA/4aa-LDH, which contains a mixture of TA^{2-} and aa^- ions, has the highest H_2 uptake. Moreover, TA/4aa-LDH has more than twice amount of H_2 uptake than that of *p*TA/3aa (0.67 wt% vs. 0.28 wt%), which contains a mixture of pTA^- and aa^- ions. On the other hand, the hydrogen uptakes of LDHs intercalated pure anion species, decrease in the order of CO_3 > TA > *p*TA ~ aa.

For physical adsorption, surface area and pore volume usually play important roles. The correlations of hydrogen uptakes at 77 K with total surface area (S_{total}) and S_{micro} are shown in Fig. 6, and those with total pore volume (V_{total}) and V_{micro} are shown in Fig. 7. The hydrogen uptakes increase with both surface areas and pore volumes. However, linear relationship can only be drawn for H_2 uptakes at 77 K with S_{micro} and V_{micro}. In the cases of total surface area and pore volume, the H_2 uptakes of TA/4aa-LDH and TA/6aa-LDH are noticeably deviated from the linear relationship. These results demonstrate that the surface area and volume of micropores are the main factors influencing hydrogen uptakes at 77 K. The H_2 uptake at 77 K per micropore surface area of LDHs materials is obtained from the slope of Fig. 6B. A value of $9.3*10^{-5}$ g/m^2 is much larger than that ($3.0*10^{-6}$ g/m^2) of MOFs reported in the literature.[3] In order to understand the interaction between the adsorbents and hydrogen, the hydrogen adsorption isotherms were taken at 77 K and 87 K, and the results for TA/4aa-LDH and *p*TA/3aa-LDH are shown in Fig. 8A. The isosteric heats of hydrogen adsorption, $Q_{ads,}$ are calculated by the Clausius-Clapeyron equation: [34,35]

$$\ln\frac{P_2}{P_1} = \frac{-Q_{ads}(T_2-T_1)}{RT_1T_2} \qquad \text{(eq.5)}$$

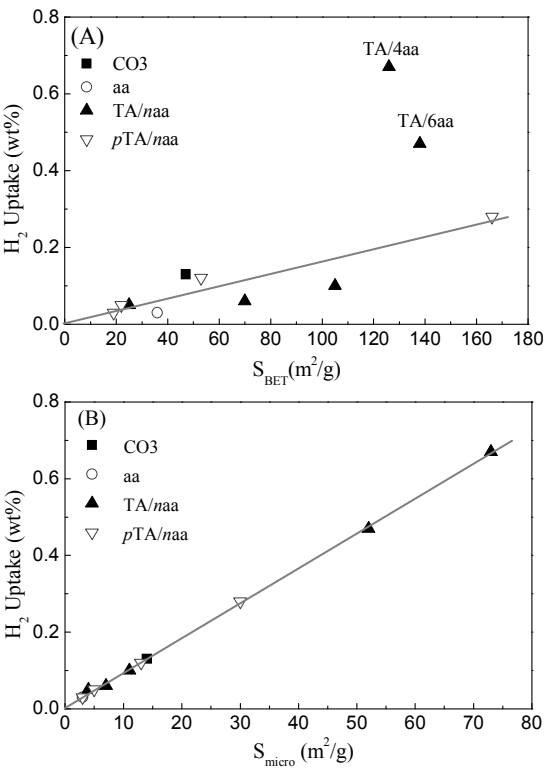

Fig. 6 Relationship between the hydrogen uptakes at 77 K/ 1 atm and (A) BET surface area, (B) microporous surface area of LDHs with different interlayer anions.

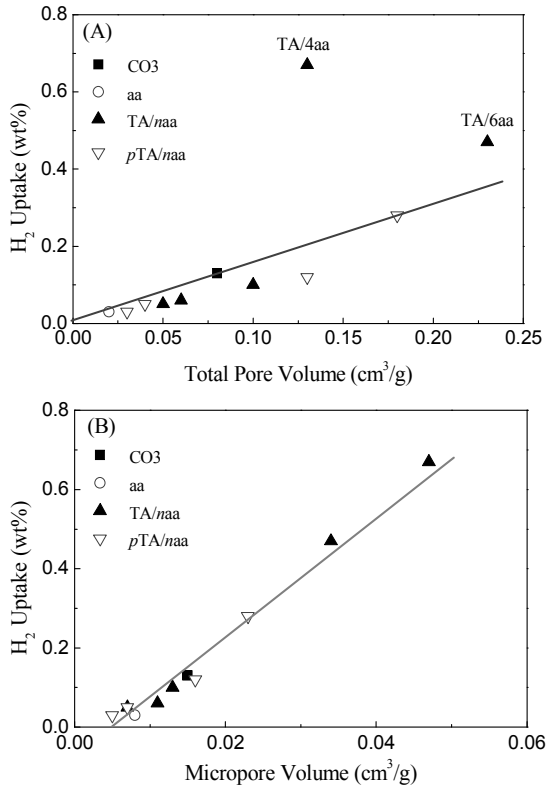

Fig. 7 Relationship between the hydrogen uptakes at 77 K/ 1 atm and (A) total pore volume, (B) microporous volume of LDHs with different interlayer anions.

The dependencies of Q_{ads} as a function of H_2 uptakes are calculated from the 77 K and 87 K isotherms, as demonstrated in Fig. 8B. The Q_{ads} values drop off sharply with the increase of H_2 uptake. The Q_{ads} values for sorption of the first layer H_2 are determined at zero coverage, and they are 21.2 and 13.6 kJ/mol for TA/4aa-LDH and *p*TA/3aa-LDH, respectively. Table 2 shows the Q_{ads} values of LDHs with various interlayer anions, and they vary in the range of 4.5-21.2 kJ/mol. It is noticed that Q_{ads} values of LDHs containing studied anions increase in the order of pTA^- ~ aa^- < CO_3^{2-} < TA^{2-}. These results infer that divalent anions seem to give higher Q_{ads} values than the monovalent anions. Furthermore, LDHs with a mixture of arylate and acetate ions have higher Q_{ads} values than those with either of the pure anions. Among them, TA/*n*aa-LDHs samples also have higher Q_{ads} values than *p*TA/*n*aa-LDHs. The physical adsorption enthalpy is of the order of the condensation enthalpy of the adsorbate, and the enthalpies are usually less than 35 kJ/mol for gases.[36,37] Moreover, the isosteric heats of hydrogen adsorption on MOFs is among 4-12 kJ/mol.[38,39] The Q_{ads} values confirm the hydrogen adsorption on LDHs is physical adsorption. Since the surface areas of LDHs increase by mixing arylate ions with acetate, the correlation between Q_{ads} and total or micropore surface areas is shown in Fig. 9. No direct relationship can be drawn in either of the plots. However, linear relationships can be found in Q_{ads} versus S_{micro} for individual TA/*n*aa-LDHs and *p*TA/*n*aa-LDHs samples. These results imply that micropore condensation is one of the key interaction forces for H_2 adsorption on LDHs materials.

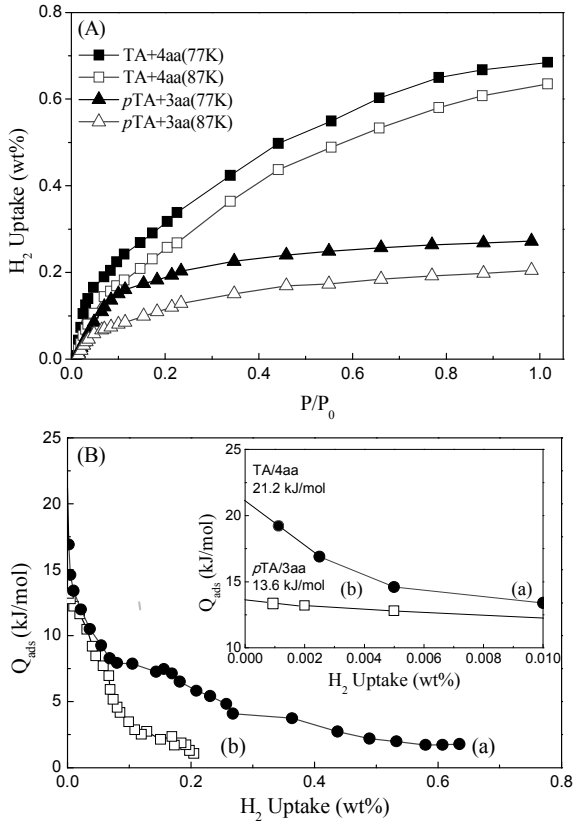

Fig. 8 (A) Low-pressure H_2 adsorption isotherms of LiAl-LDHs (a) TA/4aa at 77 K, (b) TA/4aa at 87 K, (c) *p*TA/3aa at 77 K, and (d) *p*TA/3aa-LDH at 87 K. (B) Coverage dependencies of the isosteric heat of fit of its 77 K and 87 K isotherms for (a) TA/4aa and (b) *p*TA/3aa.

It is also noticed that larger slope is obtained on the data of *p*TA/naa-LDHs than that of TA/*n*aa-LDHs, although the latter can reach higher Q_{ads} and S_{micro}. It is elucidated by that *p*TA/naa-LDHs have stronger interaction with hydrogen molecules, attributing to the denser pack of the benzene rings of pTA^- ions in the interlayer. Indeed, the slope decreases slightly with the increase in S_{micro}, which is due to the expansion of distance between pTA^- ions by mixing acetate ions in the interlayer. The hydrogen sorption at high-pressure and room temperature was measured by gravimetric method. In Fig. 10, it shows that the hydrogen uptakes increase linearly with pressure. At 100 atm, the maximal allowed pressure of the instrument, the H_2 uptakes are between 0.004-0.024 wt% for LDHs containing pure anion species, while they can reach 0.098 wt% and 0.071 wt% for TA/4aa-LDH and pTA/3aa-LDH, respectively. It is noticeable that the H_2 uptakes have not reached the maximum even at 100 atm. The correlation between the hydrogen uptake at 77 K/ 1 atm and those at 298 K/100 atm is shown in Fig. 11. A linear relationship can be drawn. Therefore, it can be derived that the hydrogen uptakes of LDHs at 298 K and 100 atm are also directly proportional to micropore surface area and pore volume, similar to the hydrogen uptakes at 77 K and 1 atm. The relation of hydrogen uptake at 298 K and 100 atm with micropore surface area and pore volume is shown in Fig. S5 (ESI†). The slope of $1.66*10^{-5}$ g/m^2 is one order higher than that of MOFs ($4.0*10^{-6}$ g/m^2) reported in the literature.[17]

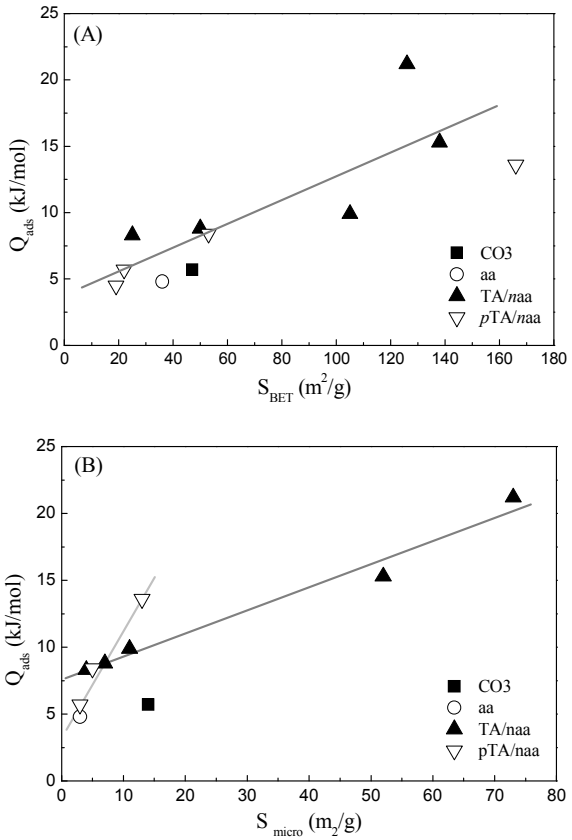

Fig. 9 Relationship between the hydrogen adsorption heats at 77 K/ 1 atm and (A) total and (B) micropore surface area.

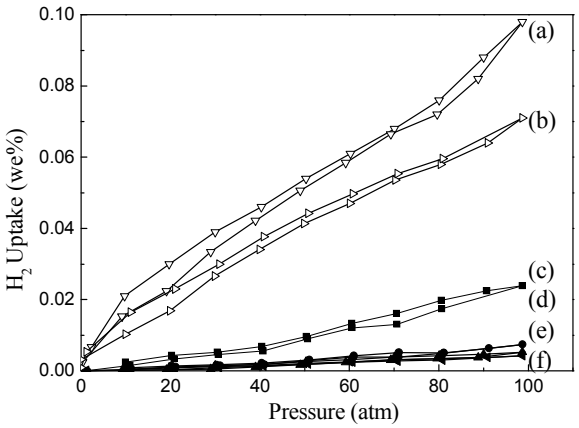

Fig. 10 H_2 adsorption isotherms of LiAl-LDHs with different interlayer anions at 298 K and 100 atm (a) TA/4aa, (b) *p*TA/3aa, (c) CO3, (d) *p*TA, (e) TA, and (f) aa.

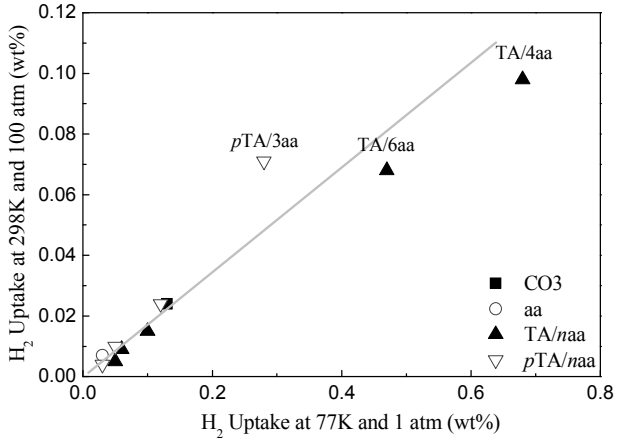

Fig. 11 Relationship between the hydrogen uptake at 77 K/1 atm and 298 K/100 atm.

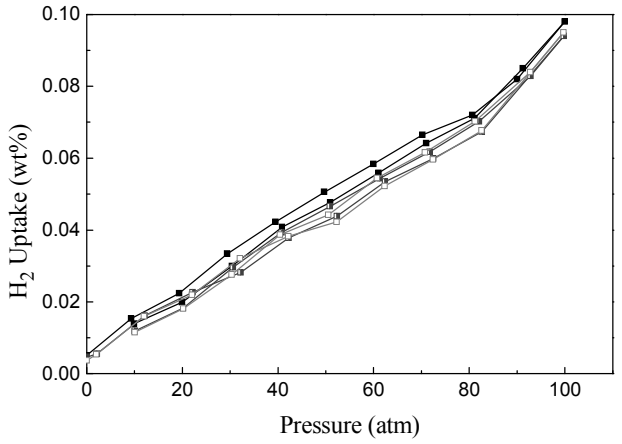

Fig. 12 The recyclability measure of LiAl-TA/4aa-LDH at 298K and 100 atm (black and solid is the first time, dark gray and center is the second time, and light gray and hollow is the third time).

These results imply that arylate intercalated LDHs can have higher H_2 adsorption capability than MOFs if the material can be prepared to have micropore surface areas as high as MOFs. Besides, the recyclability also was measured the hydrogen adsorption of LDHs after each from the third successive adsorption/ desorption cycles reusing the adsorbent. Fig. 12 shows that the hydrogen uptakes of LDH intercalated with TA/4aa anions after three cycles of adsorption/desorption still retain 96% of its 1st time uptake amount. This further confirms that LDHs materials have great potential for hydrogen adsorption.

Conclusions

Li-Al LDHs intercalated with different organic anions can be prepared by co-precipitation method. LDHs of relatively high surface areas (~150 m^2/g) were prepared with a mixture of arylate and acetate ions. The XRD patterns show that the d-spacing of TA-LDH decreases gradually from 1.41 to 0.94 nm as more and more acetate ions are introduced, attributing to the tilt of TA^{2-} anions from vertical to almost horizontal toward the basal LDH layer. For *p*TA-LDH, the larger d-spacing of 1.64 nm implies that the interlayer pTA^- ions form bilayer structure due to the strong π-π interaction. The interlayer distance of *p*TA-LDH is retained and a new layer structure is formed as acetate ions replace a portion of the interlayer pTA^- ions. The new layer structure with d-sapcing of 1.2 nm is proposed to contain bilayer with one layer of pTA^- ions and another layer of acetate ions. The replacing a portion of the interlayer arylate anions by acetate produces structural defects, and also causes the surface area and pore volume to increase for several times. Nevertheless, intercalating LDHs with a mixture of TA^{2-} and acetate ions is more effective in generating micropores than that with a mixture of pTA^- and acetate ions. When applying the LDH materials in hydrogen sorption, the materials containing mixed arylate and acetate ions show higher hydrogen uptakes than those intercalated with pure organic anions. Furthermore, LDHs containing a mixture of TA^{2-} and acetate ions have the highest H_2 uptakes. The adsorption enthalpies are found to have a direct correlation with the micropore surface area for individual *p*TA/*n*aa-LDH and TA/*n*aa-LDH samples. The highly packed benzene rings of pTA^- ions in *p*TA/*n*aa-LDH are considered to contribute to the stronger interaction between hydrogen molecules and *p*TA/*n*aa-LDH, in comparison to that with TA/*n*aa-LDH. Nevertheless, the capillary condensation is found to be one of the main interaction forces for hydrogen adsorption on these LDH materials. A linear correlation can be drawn between the hydrogen uptake and micropore surface area or pore volume. Due to the high micropore surface area and pore volume of TA/4aa-LDH, it has the maximal hydrogen adsorption capacity of 0.67wt% at 77 K/1atm and 0.098wt% at 298 K/100 atm. Furthermore, the H_2 uptake per S_{micro} of the TA/4aa-LDH material is $1.66*10^{-5}$ g/m^2, which is much larger than the value of $1.14*10^{-6}$ g/m^2 for MOFs reported in the literature.

Acknowledgement

The financial supports from Ministry of Science & Technology and Ministry of Education, Taiwan are gratefully acknowledged. Acknowledgments are also extended to Ms. S.-J. Ji, Y.-C. Chao, and J.-W. Lu of Instrumentation Center, College of Science, National Taiwan University for SEM, ICP-MS, and EA experiments.

Notes

Address: Department of Chemistry, National Taiwan University, No. 1, Sec. 4, Roosevelt Road, Taipei, 10617, Taiwan

† Electronic supplementary information (ESI) available: Detail of SEM images, TGA/DTG profiles, N_2 adsorption/desorption isotherms, relationship between high pressure hydrogen uptake and microporous surface area/ volume. See DOI: 10.1039/b000000x/

References

1) Schlapbach, L.; Zuttel, A. *Nature* **2001**, *414*, 353.
(2) Lim, K.L.; Kazemian, H.; Yaakob, Z.; Daud, W.R.W. *Chem. Eng. Technol.* **2010**, *33*, 213.
(3) Suh, M.P.; Park, H.J.; Prasad, T.K.; Lim, D.W. *Chem. Rev.* **2012**, *112*, 782.
(4) Orimo, S.I.; Nakamori, Y.; Eliseo, J.R.; Zuttel, A.; Jensen, C.M. *Chem. Rev.* **2007**, *107*, 4111.
(5) Dornheim, M.; Doppiu, S.; Barkhordarian, G.; Boesenberg, U.; Klassen, T.; Gutfleisch, O.; Bormann, R. *Scr. Mater.* **2007**, *56*, 841.
(6) Graetz, J. *Chem. Soc. Rev.* **2009**, *38*, 73.
(7) Jimenez, V.; Sanchez, P.; Diaz, J.A.; Valverde, J.L.; Romero, A. *Chem. Phys. Lett.* **2010**, *485*, 152.
(8) Hu, Y.H.; Zhang, L. *Adv. Mater.* **2010**, *22*, E117.
(9) Murray, L.J.; Dinca, M.; Long, J.R. *Chem. Soc. Rev.* **2009**, *38*, 1294.
(10) Collins, D.J.; Zhou, H.C. *J. Mater. Chem.* **2007**, *17*, 3154.
(11) Hirscher, M.; Panella, B. *Scr. Mater.* **2007**, *56*, 809.
(12) Rosi, N.L.; Eckert, J.; Eddaoudi, M.; Vodak, D.T.; Kim, J.; O'Keeffe, M.; Yaghi, O.M. *Science* **2003**, *300*, 1127.
(13) Zecchina, A.; Bordiga, S.; Vitillo, J.G.; Ricchiardi, G.; Lamberti, C.; Spoto, G.; Bjorgen, M.; Lillerud, K.P. *J. Am. Chem. Soc.* **2005**, *127*, 6361.
(14) Chung, K.H. *Energy* **2010**, *35*, 2235.
(15) Prasanth, K.P.; Raj, M.C.; Bajaj, H.C.; Kim, T.H.; Jasra, R.V. *Int. J. Hydrog. Energy* **2010**, *35*, 2351.
(16) Regli, L.; Zecchina, A.; Vitillo, J. G.; Cocina, D.; Spoto, G.; Lamberti, C.; Lillerud, K.P.; Olsbye, U.; Bordiga, S. *Phys. Chem. Chem. Phys.* **2005**, *7*, 3197.
(17) Kaye, S.S.; Dailly, A.; Yaghi, O.M.; Long, J.R. *J. Am. Chem. Soc.* **2007**, *129*, 14176.
(18) Han, S.S.; Mendoza-Cortes, J.L.; Goddard, W.A. *Chem. Soc. Rev.* **2009**, *28*, 1460.
(19) Yan, Y.; Telepeni, I.; Yang, S.; Lin, X.; Kockelmann, D.A.; Blake, A.J.; Lewis, W.; Walker, G.S.; Allan, D.R.; Barnett, S.A.; Champness, N.R.; Schroder, M. *J. Am. Chem. Soc.* **2010**, *132*, 4092.
(20) Li, Y.; Yang, R.T. *Langmuir* **2007**, *23*, 12937.
(21) Xu, Z.P.; Zhang, J.; Adebajo, M.O.; Zhang, H.; Zhou, C.H. *Appl. Clay Sci.* **2011**, *53*, 139.
(22) Newman, S.P.; Jones, W. *New J. Chem.* **1998**, *22*, 105.
(23) Shumaker, J.L.; Crofcheck, C.; Tackett, S.A.; Santillan-Jimenez, E.; Morgan, T.; Ji, Y.; Crocker, M.; Toops, T.J. *Appl. Catal. B- Environ.* **2008**, *82*, 120.
(24) Newman, S.P.; Williams, S.J.; Coveney, P.V.; Jones, W. *J. Phys. Chem. B* **1998**, *102*, 6710.
(25) Besserguenev, A.V.; Fogg, A.M.; Francis, R.J.; Price, S.J.; Ohare, D.; Isupov, V.P.; Tolochko, B.P., *Chem. Mater.* **1997**, *9*, 241.
(26) Huo, Q.S.; Margolese, D.I.; Stucky, G.D. *Chem. Mater.* **1996**, *8*, 1147.
(27) Chisem, I.C.; Jones, W. *J. Mater. Chem.* **1994**, *4*, 1737.
(28) Goh, K.-H.; Lim, T.-T.; Dong, Z. *Water Research* **2008**, *42*, 1343.
(29) Nhlapo, N.; Motumi, T.; Landman, E.; Verryn, S.M.C.; Focke, W.W. *J. Mater. Sci.* **2008**, *43*, 1033.
(30) Wang, J.; Lei, Z.; Qin, H.; Zhang, L.; Li, F. *Ind. Eng. Chem. Res.* **2011**, *50*, 7120.
(31) Seftel, E. M.; Popovici, E.; Mertens, M.; Witte, K.; Tendeloo, G.; Cool, P.; Vansant, E.F. *Micro. Meso. Mater.* **2008**, *113*, 296.
(32) Nylund, A.; Olefjord, I. *Surf. Interface Anal.* **1994**, *21*, 283.
(33) Olefjord, I.; Nylund, A. *Surf. Interface Anal.* **1994**, *21*, 290.
(34) Li, Y.; Yang, F.H.; Yang, R.T. *J. Phy. Chem. C* **2007**, *111*, 3405.
(35) Mavrandonakis, A.; Klopper, W. *J. Phy. Chem. C* **2008**, *112*, 3152.
(36) Bhatia, S.K.; Myers, A.L. *Langmuir* **2006**, *22*, 1688.
(37) Miller, M.A.; Wang, C.Y.; Merrill, G.N. *J. Phy. Chem. C* **2009**, *113*, 3222.
(38) Sokolowski, K.; Bury, W.; Justyniak, I.; Fairen-Jimenez, D.; Soltys, K.; Prochowicz, D.; Yang, S.; Schroder, M.; Lewinski, J. *Angew. Chem. Int. Ed.* **2013**, *52,* 13414.
(39) Sava, D.F.; Kravtsov, V.C.; Nouar, F.; Wojtas, L.; Eubank, J.F.; Eddaoudi, M. *J. Am. Chem. Soc.* **2008,** *130*, 3768.